Reordering of the ridge patterns of a stochastic electromagnetic field by diffraction due to an ideal slit

J. Avendaño
Departamento de Física, Escuela Superior de Física y Matemáticas, Instituto Politécnico Nacional, Codigo Postal 07738, México, Distrito Federal, Mexico

L. de la Peña
Instituto de Física, Universidad Nacional Autónoma de México, Apartado Postal 20-364, 01000 México, Distrito Federal, Mexico

(Received 23 April 2005; published 12 December 2005)

We study the behavior of scarlets of a stochastic radiation field of fixed frequency in the presence of a slit pierced on an infinitely thin metallic screen of ideal conductivity. Our methodology involves the exact solution of the Maxwell equations with appropriate boundary conditions, the only approximations being those due to the numerical procedure. Our numerical simulations show that the field is unfolded into two components, a dominant one that is disordered and a weaker one that is ordered. The former still presents scarlets although modified, while the latter exhibits a pattern of perfectly coherent diffraction. Due to the dominant character of the disordered component, the general appearance of the scattered field is stochastic; however, an underlying order exists. Our results confirm, thus, a novel effect suggested previously in the context of stochastic electrodynamics.

DOI: 10.1103/PhysRevE.72.066605 PACS number(s): 42.25.Fx, 42.25.Gy, 02.50.Ey, 02.70.Uu

I. INTRODUCTION

The problem of the scattering of electromagnetic fields by diffracting structures such as a strip grating or a rough surface has been widely studied for incident plane waves [1–4] and, more recently, for more realistic electromagnetic beam waves such as Gaussian [5], Bessel [6], Bessel-Gauss [6,7], or Hermite-Gauss [8,9] packets. These studies have been mainly motivated by the vast and important technological applications of the results [10]. Here, we revisit the problem of diffraction of a stochastic electromagnetic field of a fixed frequency. Besides our specific interest in this problem because of its possible relevance to stochastic electrodynamics, as explained at the end of the paper, we consider that the study of the diffraction of a stochastic electromagnetic field and its effect on the scarlets (see below) has an interest of its own. Our treatment has two important differences from previous studies. One is that the present calculation is exact, the only approximations being those due to the numerical procedures. The other is that we pay particular attention to the scarlets, in the following sense. A few years ago it was found that random superpositions of stochastic plane waves of fixed frequency have surprising statistical properties [11]. The common wisdom was that such random superpositions would give rise to a speckle pattern. However, numerical simulations showed unexpectedly that they form a random pattern of ridges, known as scarlets, which may be quite long, reaching sometimes 50 or even 60 wavelengths [11,12]. (An example is shown in Fig. 2 below.) Here, we study how these structures that reveal a large spatial coherence despite the disorder of the field are affected by the presence of diffracting objects. In this study, we report our results for an infinite rectangular slit pierced on a metallic infinitely thin screen of infinite conductivity and show that the diffracted field can be expressed in terms of two components, namely a stochastic one that still presents (modified) scarlets and a much more organized one, whose order is exhibited in a pattern of perfectly coherent diffraction.

Since the wavelength of the stochastic field is arbitrary in principle, it becomes necessary to use a rigorous theory to study this diffraction problem. Indeed, it is known and previous calculations with conventional fields have confirmed that for wavelengths comparable to the width of the slit, the tensor character of the electromagnetic field plays a very important role [10,13]. These effects due to polarization are neglected in the approximate diffraction scalar theories favored by the optics community [14]. Thus, one needs to resort to a rigorous theory of diffraction, which means that the only permissible approximations are those that simplify the problem (such as considering an ideal system as is done here) and the unavoidable numeric rounding errors along the calculation. Therefore, the Maxwell equations and their associated boundary conditions are here solved exactly. From among the rigorous theories of diffraction available in the specialized literature, we use the so-called modal theory [14,15], since it seems to be the one that best adapts to our problem. This means that the field inside the slit is expressed by means of a modal expansion. The fact that the calculation performed here is exact may be a point of particular interest to some of our readers.

II. FORMULATION OF THE PROBLEM

We place the diffracting structure coinciding with the plane ZX as shown in Fig. 1; this divides the empty space into two regions, the upper region $R^{(+)}=\{(x,y,z)\in\mathbb{R}^3|y>0\}$ and the bottom region $\mathbb{R}^{(-)}=\{(x,y,z)\in R^3|y<0\}$. The slit extends on the Z axis from $-\infty$ to ∞ and on the X axis from $x=0$ to $x=l$. The stochastic electromagnetic radiation field to be considered spreads downward on this device and

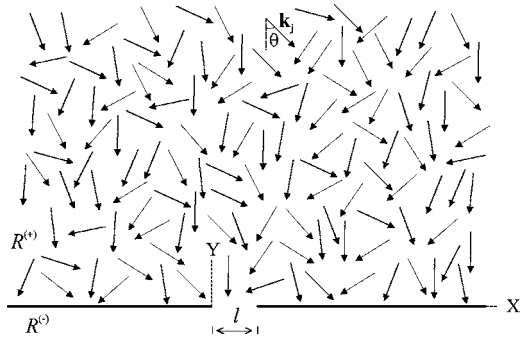

FIG. 1. Diffracting structure, plane screen of infinite conductivity (coincident with the plane *XZ*) with a rectangular slit that extends on the *Z* axis from $-\infty$ to ∞ and on the *X* axis from $x=0$ to $x=l$. This figure also shows, in a pictorial way, an incident stochastic field of fixed wavelength, which consists of a random superposition of stochastic plane waves with wave vector parallel to the plane *XY*.

consists of a random superposition of stochastic plane waves with wave vectors parallel to the plane *XY* as shown in Fig. 1. Thus, the incident field is given by [16]

$$\mathbf{E}^{\text{in}}(\mathbf{r}) = \sum_{j=1}^{N} \mathbf{E}_j e^{i(\mathbf{k}_j \cdot \mathbf{r} + \eta_j)},$$

$$\mathbf{H}^{\text{in}}(\mathbf{r}) = \sum_{j=1}^{N} \mathbf{H}_j e^{i(\mathbf{k}_j \cdot \mathbf{r} + \eta_j)}, \quad \text{with} \quad \mathbf{H}_j = \frac{\mathbf{k}_j \times \mathbf{E}_j}{\omega \mu_0}. \tag{1}$$

The wave vector of the *j*th plane wave has the form $\mathbf{k}_j = (k_{xj}, -k_{yj}, 0)$, with components

$$k_{xj} = k \sin \theta_j \quad \text{and} \quad k_{yj} = k \cos \theta_j. \tag{2}$$

The magnitude of each vector $\mathbf{k}_j$ is fixed (since the frequency is fixed), but its direction of incidence on the screen is assumed to obey a uniform statistical distribution with θ_j uniformly distributed in the interval $[-\pi/2, \pi/2]$; the phase η_j of each plane wave is uniformly distributed in the interval $[0, 2\pi)$. The amplitudes E_j and H_j follow a Gaussian distribution centered around zero and of fixed variance. In Fig. 2, we show the contour maps for a realization of this stochastic electromagnetic field, assuming that the electric field of each plane wave of the random superposition oscillates along the *Z* axis, i.e., the electric and magnetic fields have the form $\mathbf{E} = (0, 0, E_z)$ and $\mathbf{H} = (H_x, H_y, 0)$. The contour map of Fig. 2(a) corresponds to the electric field E_z^{in}, whereas Figs. 2(b) and 2(c) show the components H_x^{in} and H_y^{in} of the magnetic field, respectively. The presence of the scarlets is clearly observed. To obtain each of these figures, we have superposed 10 000 random plane waves, and the scales of the graphs were normalized to the size of the wavelength.

Our physical problem is to find the total fields **E** and **H** at each point of space in the presence of the diffracting structure. According to the condition of incidence shown in Fig. 1, the diffracted fields in the upper region of space can be written as the difference between the total field and the incident field, $\mathbf{E}_d^{(+)} = \mathbf{E} - \mathbf{E}^{\text{in}}$, $\mathbf{H}_d^{(+)} = \mathbf{H} - \mathbf{H}^{\text{in}}$, while in the bottom region, we have $\mathbf{E}_d^{(-)} = \mathbf{E}$ and $\mathbf{H}_d^{(+)} = \mathbf{H}$.

III. MATHEMATICAL FORMULATION

The description of the system is invariant under translations along the *Z* axis, since neither the stochastic incident field nor the diffracting structure change under these translations. This implies that if $\mathbf{E}(x, y, z)$ and $\mathbf{H}(x, y, z)$ are solutions of the Maxwell equations, $\mathbf{E}(x, y, z')$ and $\mathbf{H}(x, y, z')$ will be solutions for any $z' \neq z$. Uniqueness of the solution implies then that the electromagnetic field should be independent of the *z* coordinate. Under this condition, the Maxwell equations can be decomposed into two independent sets of equations [15,17]. One set corresponds to the transverse electric (TE) polarization, which contains the components E_z, H_x, and H_y of the electromagnetic field,

$$\nabla^2 E_z + k^2 E_z = 0, \tag{3a}$$

$$H_x = -\frac{i}{\omega \mu_0} \frac{\partial E_z}{\partial y}, \tag{3b}$$

$$H_y = \frac{i}{\omega \mu_0} \frac{\partial E_z}{\partial x}. \tag{3c}$$

Here $k = \omega \sqrt{\mu_0 \epsilon_0} = 2\pi/\lambda$ is the magnitude of the wave vector, ϵ_0 and μ_0 are the electric permittivity and magnetic permeability of the vacuum, respectively. The second set of equations corresponds to the transverse magnetic (TM) polarization, described by the components H_z, E_x, and E_y, so that

$$\nabla^2 H_z + k^2 H_z = 0, \tag{4a}$$

$$E_x = \frac{i}{\omega \epsilon_0} \frac{\partial H_z}{\partial y}, \tag{4b}$$

$$E_y = -\frac{i}{\omega \epsilon_0} \frac{\partial H_z}{\partial x}. \tag{4c}$$

These sets of equations together imply that the polarization is conserved, i.e., if the stochastic incident field possesses polarization TE or TM, the diffracted field will also have polarization TE or TM, respectively. We denote, thus, by $U(x, y)$ the component E_z in the TE case or H_z in the TM case and look for solutions to the Helmholtz equations (3a) or (4a) that satisfy the following conditions: (1) the electromagnetic field is bounded for large *y* (boundary condition at infinity), and (2) the stochastic incident field propagates downward in the upper region (initial condition of incidence).

It is convenient to keep the variable *y* in the configuration space, but to perform a Fourier transformation in the variable *x*, so that the solution in $R^{(+)}$ can be expressed as

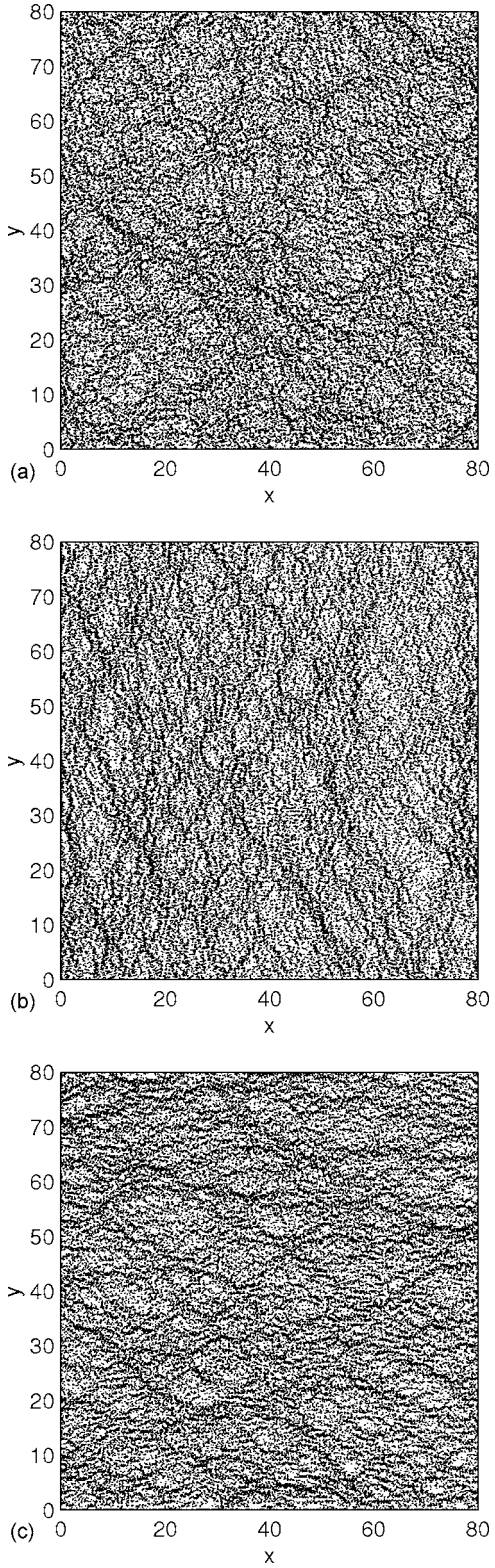

FIG. 2. *XY* contour map of an incident stochastic electromagnetic field with polarization perpendicular to the plane *XY*, over a region of 80 wavelengths on each side. The stochastic field is a superposition of 10 000 plane waves, each with a random orientation **k** in the semicircle of incidence, a random phase shift, and a Gaussian random amplitude. Panel (a) corresponds to the electric field E_z^{in}, (b) shows the component H_x^{in} of the magnetic field, and (c) the component H_y^{in}.

$$U(x,y) = \frac{1}{\sqrt{2\pi}}\int_{-\infty}^{+\infty} I(\alpha)e^{i[\alpha x-\beta(\alpha)y]}d\alpha + \frac{1}{\sqrt{2\pi}}\int_{-\infty}^{+\infty} R(\alpha)e^{i[\alpha x+\beta(\alpha)y]}d\alpha \equiv U^{(+)}(x,y), \tag{5a}$$

whereas in $R^{(-)}$, we have

$$U(x,y) = \frac{1}{\sqrt{2\pi}}\int_{-\infty}^{+\infty} T(\alpha)e^{i[\alpha x-\beta(\alpha)y]}d\alpha \equiv U^{(-)}(x,y). \tag{5b}$$

Here and in the following, the + and − signs refer to the upper and lower half planes, respectively. Further $\beta(\alpha) = \sqrt{k^2-\alpha^2}$ is a real number $[\beta(\alpha)\geqslant 0]$ for traveling waves, and a purely imaginary number $[-i\beta(\alpha)\geqslant 0]$ for evanescent waves. $I(\alpha)$ is the spectral distribution of amplitudes of the stochastic incident field. Since $U^{(+)}(x,y)$ is bounded for large y, we must have

$$I(\alpha) = 0 \;\forall\; |\alpha| > k. \tag{5c}$$

Our problem has been reduced to the determination of $R(\alpha)$ and $T(\alpha)$, the spectral distributions of the backward (reflected) and downward (transmitted) diffracted fields, respectively.

A. TM case

In this case, $U(x,y)$ is the tangential (to the metallic screen) component of the magnetic field H_z. The boundary condition of the electromagnetic field at $y=0$ (on the diffracting structure) implies that the tangential component of the magnetic field is continuous on the slit

$$H_z^{(+)}(x,0) = H_z^{(-)}(x,0), \quad \forall\; x \in (0,l), \tag{6}$$

while the tangential component of the electric field E_x is continuous on both the screen and the slit, so that from Eq. (4b) it follows that

$$\frac{\partial H_z^{(+)}}{\partial y}(x,0) = \frac{\partial H_z^{(-)}}{\partial y}(x,0), \quad \forall\; x \in (-\infty,+\infty). \tag{7}$$

Since the tangential electric field E_x is null on the metallic screen, we have the additional conditions

$$\frac{\partial H_z^{(+)}}{\partial y}(x,0) = 0,$$

$$\frac{\partial H_z^{(-)}}{\partial y}(x,0) = 0, \quad \forall\; x \in (-\infty,0]\cup[l,+\infty). \tag{8}$$

From Eqs. (5a) and (5b) together with Eq. (7), it follows that the spectral distributions $I(\alpha)$, $R(\alpha)$, and $T(\alpha)$ are related by

$$I(\alpha) = R(\alpha) + T(\alpha). \tag{9}$$

This result allows us to cast the second term of the right-hand side (rhs) of Eq. (5a) [backwardly diffracted field, $H_{z,d}^{(+)}(x,y)$] into the form

$$H_{z,d}^{(+)}(x,y) = \frac{1}{\sqrt{2\pi}}\int_{-\infty}^{+\infty} R(\alpha)e^{i[\alpha x+\beta(\alpha)y]}d\alpha$$
$$= \frac{1}{\sqrt{2\pi}}\int_{-k}^{+k} I(\alpha)e^{i[\alpha x+\beta(\alpha)y]}d\alpha$$
$$- \frac{1}{\sqrt{2\pi}}\int_{-\infty}^{+\infty} T(\alpha)e^{i[\alpha x+\beta(\alpha)y]}d\alpha$$
$$\equiv H_{z,sr}^{(+)}(x,y) + H_{z,pd}^{(+)}(x,y). \quad (10)$$

In writing the second equality, we used condition (5c). We see that the backwardly diffracted field can be separated into two parts: the one denoted by $H_{z,sr}^{(+)}$ is the specular reflection of the stochastic incident field H_z^{in} represented by the first term on the rhs of Eq. (5a), which exists even in the absence of the slit; the other one, denoted by $H_{z,pd}^{(+)}$, represents a purely backward diffraction field and is due to the presence of the slit. The specular reflection field oscillates in phase with the stochastic incident field as follows from Eqs. (10) and (5a), while the backwardly diffracted field experiences a phase shift of π radians with respect to the upwardly diffracted field, see Eqs. (10) and (5b).

The Helmholtz equation for the field H_z within the slit becomes an eigenvalue problem with Neumann boundary conditions, since at the edges of the slit $\forall\ x \in (0,l)$, we have

$$\frac{d^2H_z(x,0)}{dx^2} + k^2H_z(x,0) = 0 \quad \text{with } \frac{\partial H_z}{\partial x}(0,0) = 0,$$

$$\frac{\partial H_z}{\partial x}(l,0) = 0. \quad (11)$$

The general solution to these equations is a linear superposition of the eigenfuctions (usually called modal expansion),

$$H_z(x,0) = \sum_n a_n\phi_n(x), \quad (12a)$$

where

$$\phi_n(x) = \begin{cases} \cos(\pi nx/l) & \text{if } x \in (0,l) \\ 0 & \text{if } x \notin (0,l) \end{cases}, \quad n \in \mathbb{N}\cup\{0\}. \quad (12b)$$

The completeness property of the eigenfuctions $\phi_n(x)$ allows us to write the normal derivative $\partial H_z/\partial y$ inside the slit as given by Eq. (7) in the form

$$\frac{\partial H_z^{(+)}}{\partial y}(x,0) = \frac{\partial H_z^{(-)}}{\partial y}(x,0) = \sum_{n=0}^{\infty} q_n\phi_n(x), \quad \forall\ x \in (0,l). \quad (13)$$

A Fourier analysis of this equation allows us to write the spectral distributions $R(\alpha)$ and $T(\alpha)$ as functions of the modal coefficients q_n

$$I(\alpha) - R(\alpha) = T(\alpha) = \sum_{n=0}^{\infty} q_n\frac{i\tilde{\phi}_n(\alpha)}{\beta(\alpha)}, \quad (14a)$$

where

$$\tilde{\phi}_n(\alpha) = \frac{i\alpha}{\sqrt{2\pi}}\frac{1-(-1)^ne^{-i\alpha l}}{(\pi n/l)^2-\alpha^2} \quad (14b)$$

is the Fourier transform of $\phi_n(x)$. In its turn, the continuity of the magnetic field H_z on the slit Eq. (6) allows us to define a function $f(x)$ identical to zero by means of

$$f(x) \equiv H_z^{(+)}(x,0) - H_z^{(-)}(x,0) = 0, \quad \forall\ x \in (0,l), \quad (15)$$

which can be expressed also as a superposition of the eigenfunctions in the form $f(x)=\Sigma f_n\phi_n(x)$, where the coefficients of the expansion f_n are all equal to zero. Using now the Parserval-Plancherel theorem, we obtain

$$f_n = \langle\tilde{\phi}_n(\alpha),\tilde{f}(\alpha)\rangle = \int_{-\infty}^{+\infty}\tilde{\phi}_n^*(\alpha)\tilde{f}(\alpha)d\alpha = 0,$$

$$\forall\ n \in \mathbb{N}\cup\{0\}. \quad (16)$$

Here, $\tilde{\phi}_n(\alpha)$ and $\tilde{f}(\alpha)$ are the Fourier transforms of $\phi_n(x)$ and $f(x)$, respectively.

With the help of Eqs. (5a), (5b), (14a), and (15), Eq. (16) acquires the form

$$\sum_{m=0}^{\infty}\left\langle\tilde{\phi}_m(\alpha),\frac{2i\tilde{\phi}_n(\alpha)}{\beta(\alpha)}\right\rangle q_m = \langle\tilde{\phi}_m(\alpha),2I(\alpha)\rangle,$$

$$\forall\ n \in \mathbb{N}\cup\{0\}, \quad (17)$$

or, written in matrix form,

$$\begin{pmatrix} Q_{00} & Q_{01} & \cdots \\ Q_{10} & Q_{11} & \cdots \\ \vdots & \vdots & \ddots \end{pmatrix}\begin{pmatrix} q_0 \\ q_1 \\ \vdots \end{pmatrix} = \begin{pmatrix} P_0 \\ P_1 \\ \vdots \end{pmatrix}, \quad (18)$$

where the matrix elements are given by

$$Q_{mn} = \left\langle\tilde{\phi}_m(\alpha),\frac{2i\tilde{\phi}_n(\alpha)}{\beta(\alpha)}\right\rangle$$
$$= \frac{i}{\pi}\int_{-\infty}^{+\infty}\frac{\alpha^2[1-(-1)^me^{i\alpha l}][1-(-1)^ne^{-i\alpha l}]}{\sqrt{k^2-\alpha^2}(\pi^2m^2/l^2-\alpha^2)(\pi^2n^2/l^2-\alpha^2)}d\alpha, \quad (19a)$$

$$P_m = \langle\tilde{\phi}_m(\alpha),2I(\alpha)\rangle$$
$$= -2ik\sum_{j=1}^{N}H_j\frac{e^{i\eta_j}\sin\theta_j[1-(-1)^me^{ikl\sin\theta_j}]}{\pi^2m^2/l^2-k^2\sin^2\theta_j}. \quad (19b)$$

The latter expression can be evaluated directly, and its derivation is shown in Appendix A. However, the Q_{mn} will be expressed in terms of the eigenfunctions and evaluated numerically. Once all the matrix elements have been determined, the modal coefficients are calculated multiplying both

sides of Eq. (18) by Q^{-1}, and from these results, the spectral distributions $R(\alpha)$ and $T(\alpha)$ are determined using Eq. (14a). This procedure allows us to determine the total electromagnetic field at all points in space by means of Eqs. (5) and (4). In this way, the TM case is completely solved.

B. TE case

In the TE case, $U(x,y)$ in Eqs. (5a) and (5b) is the component E_z of the electric field, so the boundary conditions applied to the tangential components of the electromagnetic field at the interface become

$$E_z^{(+)}(x,0) = E_z^{(-)}(x,0), \quad \forall\ x \in (-\infty,\infty), \tag{20}$$

$$\frac{\partial E_z^{(+)}}{\partial y}(x,0) = \frac{\partial E_z^{(-)}}{\partial y}(x,0), \quad \forall\ x \in (0,l). \tag{21}$$

The supplementary condition is now

$$E_z^{(+)}(x,0) = 0, \quad E_z^{(-)}(x,0) = 0, \quad \forall\ x \in (-\infty,0] \cup [l,+\infty). \tag{22}$$

Thus inside the slit, we have a Dirichlet eigenvalue problem on the boundary, with $E_z(0,0)=0$, $E_z(l,0)=0$, so the electric field can be expressed in the form

$$E_z(x,0) = \sum_n b_n \phi_n(x), \tag{23a}$$

where the eigenfunctions are now

$$\phi_n(x) = \begin{cases} \sin(\pi n x/l) & \text{if } x \in (0,l) \\ 0 & \text{if } x \notin (0,l) \end{cases}, \quad n \in \mathbb{N}. \tag{23b}$$

The mode $n=0$ has been suppressed to avoid the uninteresting identically null solution.

The x-Fourier analysis of the continuity condition Eq. (20) applied to Eqs. (23) shows that the spectral distributions $I(\alpha)$, $R(\alpha)$, and $T(\alpha)$ are related by

$$I(\alpha) + R(\alpha) = T(\alpha) = \sum_{n=1}^{\infty} b_n \tilde{\phi}_n(\alpha), \tag{24a}$$

where

$$\tilde{\phi}_n(\alpha) = \frac{n\sqrt{\pi}}{\sqrt{2}l} \frac{1-(-1)^n e^{-i\alpha l}}{(\pi n/l)^2 - \alpha^2} \tag{24b}$$

is the Fourier transform of $\phi_n(x)$. The backwardly diffracted field is now

$$\begin{aligned} E_{z,d}^{(+)}(x,y) &= -\frac{1}{\sqrt{2\pi}} \int_{-k}^{+k} I(\alpha) e^{i[\alpha x + \beta(\alpha) y]} d\alpha \\ &\quad + \frac{1}{\sqrt{2\pi}} \int_{-\infty}^{+\infty} T(\alpha) e^{i[\alpha x + \beta(\alpha) y]} d\alpha \\ &\equiv E_{z,sr}^{(+)}(x,y) + E_{z,pd}^{(+)}(x,y), \end{aligned} \tag{25}$$

where once more condition (5c) has been used. We see that in this case, the specular reflected field oscillates in phase opposition to the incident field (as is well known), while the purely backwardly diffracted field oscillates in phase with the upwardly diffracted field, as follows from Eq. (5b).

In analogy to the TM case, the continuity condition for $\partial E_z/\partial y$ on the slit leads to the matrix equation

$$\begin{pmatrix} B_{11} & B_{12} & \cdots \\ B_{21} & B_{22} & \cdots \\ \vdots & \vdots & \ddots \end{pmatrix} \begin{pmatrix} b_1 \\ b_2 \\ \vdots \end{pmatrix} = \begin{pmatrix} S_1 \\ S_2 \\ \vdots \end{pmatrix}, \tag{26}$$

where the matrix elements are given by the expressions

$$\begin{aligned} B_{mn} &= \langle \tilde{\phi}_m(\alpha), i\beta(\alpha)\tilde{\phi}_n(\alpha) \rangle \\ &= \frac{2inm\pi}{l^2} \int_{-\infty}^{+\infty} \frac{\sqrt{k^2-\alpha^2}[1-(-1)^n e^{i\alpha l}][1-(-1)^m e^{-i\alpha l}]}{[(\pi n/l)^2 - \alpha^2][(\pi m/l)^2 - \alpha^2]} d\alpha, \end{aligned} \tag{27a}$$

$$\begin{aligned} S_m &= \langle \tilde{\phi}_m(\alpha), 2i\beta(\alpha) I(\alpha) \rangle . \\ &= \frac{2i\pi mk}{l} \sum_{j=1}^{N} E_j \frac{e^{i\eta_j \cos\theta_j}[1-(-1)^m e^{ikl\sin\theta_j}]}{(\pi m/l)^2 - k^2 \sin^2\theta_j}. \end{aligned} \tag{27b}$$

[See Appendix A for the explicit derivation of Eq. (27b).] We arrive at a situation similar to that of the TM case, where the matrix elements S_m can be calculated directly and B_{mn} are to be evaluated numerically. With this the TE problem is solved, since it suffices to multiply Eq. (26) by the inverse of matrix B in order to obtain the modal coefficients b_n. These are then used to calculate the spectral distributions $R(\alpha)$ and $T(\alpha)$ using Eqs. (24), and the total electromagnetic field at any point of space is thus obtained from Eqs. (5) and (4).

IV. NUMERICAL IMPLEMENTATION

The first step for the numerical solution of the matrix equations (18) and (26) is to replace the infinite matrices Q and B with finite ones. We implemented this using a convergence criterion, by which the numerical stability of the results was checked as the number of eigenmodes in the expansions Eqs. (12), (13) and (23a) was increased. The numerical evaluation of the matrix elements Q_{mn} [Eq. (19a)] and B_{mn} [Eq. (27a)] is very delicate and cumbersome, due to the violent oscillatory behavior of their integrands. This problem was solved by an appropriate change of the integration path into the complex plane, as shown in Ref. [5] for the TE case. During the convergence process, the criteria of energy balance and reciprocity relations were also checked (see Appendix B). In our calculations both criteria were always substantiated, the former to three significant digits and the latter to an accuracy better than 10^{-5}, even when the use of a small number of modes leads to erroneous results. Thus, these criteria are very important to check the numerical code, but cannot be used to control the results. The required number of terms in the modal expansions depends critically on the angle of incidence of the field impinging on the slit, as well as on the optogeometric parameter λ/l. This point is just

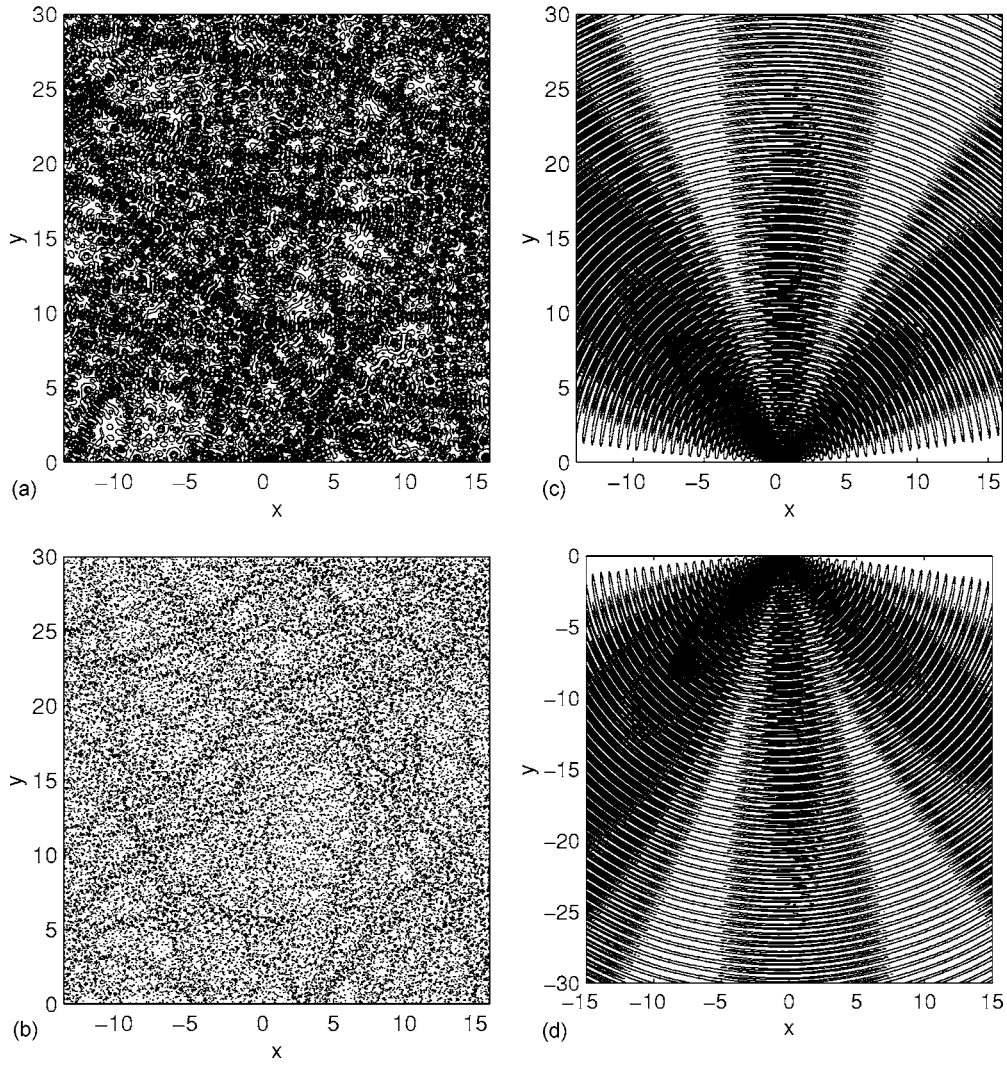

FIG. 3. Shows the diffraction process for a specific realization of the stochastic electromagnetic field with TE polarization $[\mathbf{E}=(0,0,E_z)]$ and wavelength normalized to the width of the slit. Here and in the following figures, all distances are measured relative to the width of the slit. Panel (a) shows the corresponding XY contour map of the incident electric field (E_z^{in}), (b) is the XY contour map of the backward diffracted electric field, (c) corresponds to the XY contour map of purely backwardly diffracted electric field, and (d) shows the XY contour map of the upwardly diffracted electric field.

the weakness of the modal theory, since it may lead to unstable or erroneous results if an important mode happens to be omitted from the computation. In the specialized literature, it is asserted that this number rarely exceeds 15 for a plane wave or a beam wave arriving at an angle close to normal incidence [5]. However, in our simulations, we have found that when the incidence angle is larger than 50° or 60° with respect to the normal, the number of terms should be increased up to at least 80 or 90 to attain the required precision. In our random superpositions, we have incidence angles of all values, since they follow a uniform distribution in the interval $[-\pi/2,\pi/2]$. Therefore, in the simulations, we used a minimum number of 50 terms. Once the modal coefficients had been calculated subject to the control criteria, the diffracted fields were evaluated by means of the Fourier transform given by Eqs. (5), with Eq. (14a) or Eq. (24a) for the TM or TE case, respectively. The integrand of these integral transforms has violent oscillations in the vicinity of $\alpha=k$ when $|\alpha|<k$, so in this region it is important to use a technique of adaptive quadrature in the integration procedure. In the region $|\alpha|>k$ (that of evanescent waves), the integrand goes quickly to zero as the field is evaluated farther from the slit. In our calculations, the integration interval was initially limited to $[-\zeta k,\zeta k]$, where ζ is a positive real scaling factor. The convergence process in the evaluations of the Fourier transforms was checked by enlarging the range of the variable α by means of the scale parameter ζ; a typical maximum value was about $\zeta=5$.

V. EXAMPLES OF A NUMERICAL SIMULATION

As a first example of the results obtained with the described procedure, in Fig. 3(a), we show the XY contour map of the electric component of a realization of the stochastic incident field with TE polarization. The wavelength in units of the length of the slit, which extends from 0 to 1 on the X

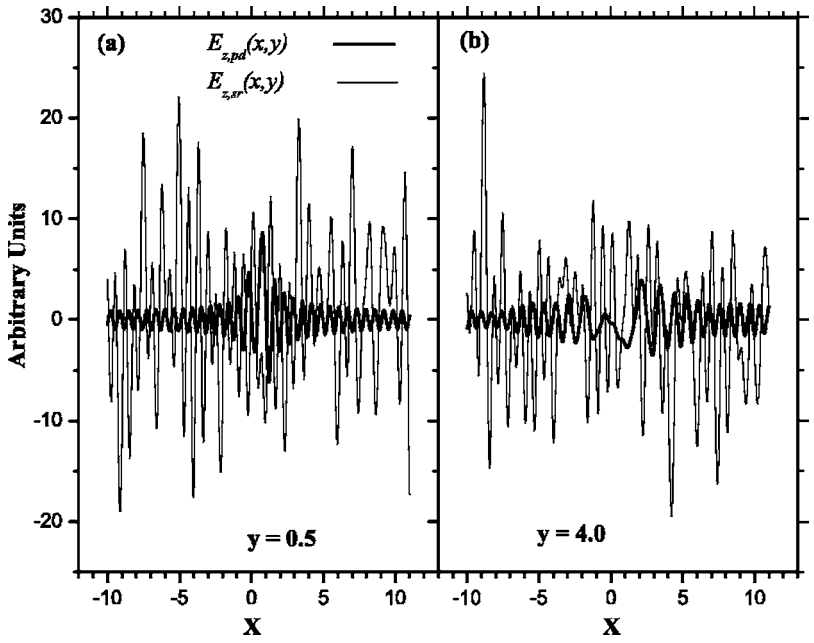

FIG. 4. Comparision between the specular reflection field $[E_{z,sr}(x,y)$, which is stochastic] and the well ordered purely backwardly diffracted field $[E^{(+)}_{z,pd}(x,y)]$ at different distances (y) of the screen: (a) at $y=0.5$ and (b) at $y=4.0$. The magnitude of the fields (vertical axis) is given in arbitrary units.

axis, is $\lambda=0.628\,32$ ($k=2\pi/\lambda=10$). Once more the scarlets are clearly visible. Figure 3(b) shows the contour map of the backward diffracted electric field $E^{(+)}_{z,d}(x,y)$; comparing this figure with the previous one, we notice that the distribution of the electric scarlets is modified by the presence of the diffracting structure, albeit no clear evidence of the presence of the slit is noticeable. Figure 3(c) shows the contour map of the purely backwardly diffracted electric field $E^{(+)}_{z,pd}(x,y)$; here, we observe that a perfectly ordered pattern of coherent diffraction emerges in spite of the stochasticity of the incoming field (we recall that here the specular reflected electric field has been subtracted from the diffracted electric field). Figure 3(d) shows the contour map of the upwardly diffracted electric field $E^{(-)}_{z,d}(x,y)$; here, only an ordered diffraction pattern appears since in region $R^{(-)}$ there is no stochastic incident field. Of course the stochastic appearance of the diffracted field in reflection (backwardly diffracted) in Fig. 3(b) is due to the fact that in $R^{(+)}$ both the specular reflection that is stochastic [according to Eq. (10) it has the same general characteristics of the incident field], and the well ordered purely backwardly diffracted field [Eq. (10) and Fig. 3(c)] contribute to the diffraction field; however, the dominant component is the stochastic one (specular reflection), as one can readily observe from Fig. 4, where a comparison is made of both fields at different places in front of the screen at $y=0.5$ and $y=4.0$. From this figure, we also observe that the magnitude of the ordered field swiftly diminishes as one goes away from the diffracting structure, while the specular reflection is sustained. Thus, any possible effect due to diffraction should occur in the proximity (a few wavelengths) of the slit.

Similar qualitative results are obtained changing the initial conditions of the incident field, such as the polarization or the specific realization of the disorder, as well as the optogeometric parameter λ/l. For example, Fig. 5 shows the diffraction in reflection and in transmission for a stochastic field impacting with polarization TM, the wavelength and the realization of the disorder being the same as in the previous case. Figures 5(a) and 5(b) show the contour maps of the magnetic component H_z. When comparing the graphs of this simulation with those corresponding to the previous case, one observes, in a qualitative way, the effects of the tensor character of the stochastic incident electromagnetic field. In a forthcoming paper, we present a quantitative analysis of the effects of all these parameters on the diffracted field and extend the study to more than one slit; here, we restrict ourselves to presenting just the qualitative aspects of this behavior by showing that the slit works somehow as a corrective mechanism of the stochastic field.

VI. CONCLUSION

The main conclusion that one can draw from the above analysis is of a qualitative character, namely that a stochastic electromagnetic radiation field in the presence of a diffracting structure contains two components: a stochastic one that still presents scarlets and another much more organized one, whose order is exhibited in a pattern of perfectly coherent diffraction. The dominant component is the stochastic one, with the result that the general appearance of the diffracted field is stochastic. This qualitative behavior is quite robust, since it is manifested independently of the value of the parameters that characterize the stochastic field, such as the specific realization of the disorder, the polarization or the size of the optogeometric parameter λ/l, and even the presence of the incident field in whole space, and not restricted to the $R^{(+)}$ region, as was done here for clarity of the exposition. Thus, we are confirming the existence of a novel effect suggested elsewhere several years ago [20], namely that underlying the scarlets of a stochastic field in presence of a diffracting structure, a perfectly ordered field exists, manifested in a coherent pattern of diffraction.

From a conceptual point of view and in a more speculative vein, we may add the following remark. The disclosed

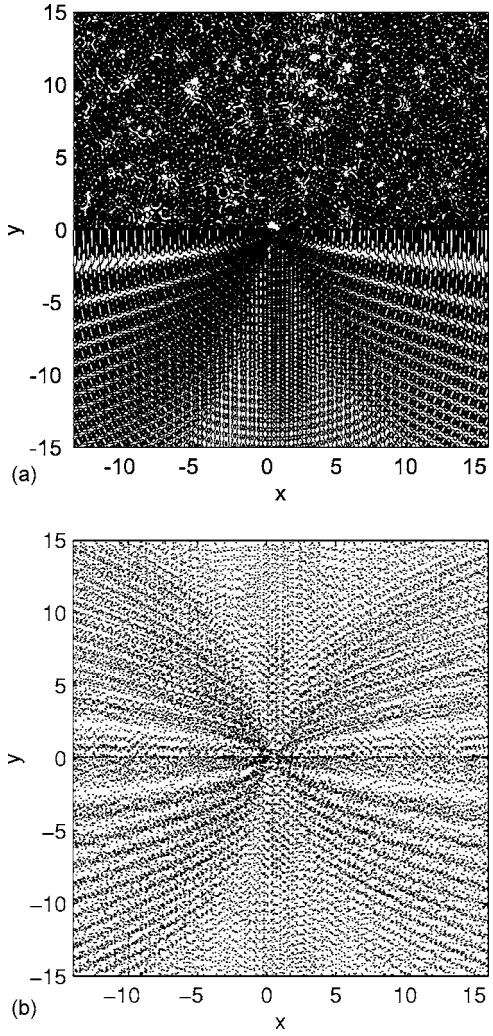

FIG. 5. Diffraction in reflection and in transmission for a stochastic electromagnetic field with TM polarization $[\mathbf{H}=(0,0,H_z)]$. The optogeometric parameters and those of the specific realization of the field are the same of Fig. 3. Panel (a) shows in the upper half the XY contour map of the backward diffracted magnetic field H_z, while in the lower half, the upward magnetic field H_z. Panel (b) corresponds to the XY contour map of the purely backward and upward diffracted magnetic field.

behavior of the field may be of importance for a physical understanding of the origin of the phenomenon of quantum diffraction of matter. Indeed, during the last decades there has been substantial investigation on the hypothesis that the quantum behavior of matter can have its origin in the interaction of matter with the vacuum radiation field [20–23]. This universal background field is called the zero-point field, because it is supposed to exist even at zero absolute temperature and also because its properties are close to those of the vacuum or zero-point field of quantum electrodynamics [20–25]. According to the present results, this stochastic zero-point field in presence of a diffracting structure acquires an underlying coherent diffraction component. Would electrons immersed in this vacuum field somehow follow the ordered diffraction pattern, filtering out the disordered component, perhaps due just to its disorder? Such a possibility would open the door to an explanation with deep physical meaning of the diffraction of matter. This is an issue that needs much more investigation to determine its potentiality, but the prospect is certainly worth the effort.

ACKNOWLEDGMENT

J.A. would like to thank the Instituto de Física UNAM for its hospitality where much of the present work was done.

APPENDIX A

Let us denote the stochastic incident field by $U^{\mathrm{in}}(x,y)$; in the case of TE or TM polarization, $U^{\mathrm{in}}(x,y)=E_z^{\mathrm{in}}(x,y)$ or $U^{\mathrm{in}}(x,y)=H_z^{\mathrm{in}}(x,y)$, respectively. Then, $U^{\mathrm{in}}(x,y)$ is the random superposition of plane waves with the statistical characteristics defined in Sec. III, so

$$U^{\mathrm{in}}(x,y)=\sum_{j=1}^{N} U_j \exp[i(xk\sin\theta_j - yk\cos\theta_j + \eta_j)]. \tag{A1}$$

Denoting by $\tilde{U}^{\mathrm{in}}(\alpha,y)$ the x-Fourier transform of the $U^{\mathrm{in}}(x,y)$ field, we have

$$U^{\mathrm{in}}(x,y)=\frac{1}{\sqrt{2\pi}}\int_{-\infty}^{+\infty}\tilde{U}^{\mathrm{in}}(\alpha,y)e^{i\alpha x}d\alpha, \tag{A2}$$

so that

$$\begin{aligned}\tilde{U}^{\mathrm{in}}(\alpha,y)&=\sum_{j=1}^{N}\sqrt{2\pi}U_j e^{i\eta_j}\delta(\alpha-k\sin\theta_j)e^{-iky\cos\theta_j}\\&\equiv I(\alpha)e^{-iy\beta(\alpha)},\end{aligned} \tag{A3}$$

where $I(\alpha)$ is the spectral distribution of the incident field introduced in Eq. (5a).

For the TM case, the matrix elements P_n, Eq. (19b), can now be readily evaluated. Sustituting $\tilde{\phi}_n$ from Eq. (14b) and $I(\alpha)$ from Eq. (A3) in Eq. (19b), we obtain, in an immediate way,

$$\begin{aligned}P_n&=2\int_{-\infty}^{+\infty}\tilde{\phi}_n^{*}(\alpha)I(\alpha)d\alpha\\&=2\int_{-\infty}^{+\infty}\frac{-i\alpha}{\sqrt{2\pi}}\frac{1-(-1)^n e^{i\alpha l}}{\frac{\pi^2 n^2}{l^2}-\alpha^2}\sum_{j=1}^{N}\sqrt{2\pi}U_j e^{i\eta_j}\\&\quad\times\delta(k\sin\theta_j-\alpha)e^{i[\beta(\alpha)-k\cos\theta_j]y}d\alpha,\end{aligned} \tag{A4}$$

which after performing the integration acquires the form

$$P_n=-2ik\sum_{j=1}^{N}H_j\frac{e^{i\eta_j}\sin\theta_j[1-(-1)^n e^{ikl\sin\theta_j}]}{\frac{\pi^2 n^2}{l^2}-k^2\sin^2\theta_j}. \tag{A5}$$

In a similar manner for the TE case, the direct substitution of Eqs. (24b) and (A3) for $\tilde{\phi}_n$ and $I(\alpha)$, respectively, in Eq. (27b) allows us to obtain for S_n, the expressions

$$S_n = 2i\int_{-\infty}^{+\infty} \tilde{\phi}_n^*(\alpha)\beta(\alpha)I(\alpha)d\alpha$$

$$= \frac{2i\pi nk}{l}\sum_{j=1}^{N} E_j \frac{e^{i\eta_j}\cos\theta_j[1-(-1)^n e^{ikl\sin\theta_j}]}{\frac{\pi^2 n^2}{l^2} - k^2\sin^2\theta_j}. \quad \text{(A6)}$$

APPENDIX B

Applying the Cadilhac-Maystre-Mata lemma [17–19] to the Pointing vector, we may write the conservation of energy theorem in the form

$$\int_{-k}^{k}\beta(\alpha)|I(\alpha)|^2 d\alpha = \int_{-k}^{k}\beta(\alpha)|R(\alpha)|^2 d\alpha + \int_{-k}^{k}\beta(\alpha)|T(\alpha)|^2 d\alpha \quad \text{(B1)}$$

that simply states that the diffracted and incident energies are equal.

However, in our problem, the expression (B1) has serious complications, because the spectral distribution $I(\alpha)$ of the incident radiation is a random superposition of delta functions [see Eq. (A3)], so the first integral in Eq. (B1) is divergent. This problem can be circumvented substituting Eq. (9) for the TM case or Eq. (24a) for the TE case in Eq. (B1), so that the divergencies cancel out. In this form, we obtain the following expression for the energy balance condition:

$$\int_{-k}^{k}\beta(\alpha)|T(\alpha)|^2 d\alpha - \mathrm{Re}\left\{\int_{-k}^{k}\beta(\alpha)T(\alpha)I^*(\alpha)d\alpha\right\} = 0. \quad \text{(B2)}$$

Using the explicit expression for $I(\alpha)$ given in Eq. (A3), the balance of energy can be recast into the form

$$\int_{-k}^{k}\beta(\alpha)|T(\alpha)|^2 d\alpha - \sum_{j=1}^{N}\sqrt{2\pi}U_j k\cos\theta_j \times \mathrm{Re}\{e^{-i\eta_j}T(k\sin\theta_j)\} = 0. \quad \text{(B3)}$$

$T(k\sin\theta_j)$ is the upwardly diffracted spectral distribution at the random direction defined by θ_j.

Another important application of the lemma is the establishment of reciprocity relations, which are just those obtained by demanding time reversal symmetry for the diffraction problem. The direct application of the lemma to our physical problem leads to reciprocity by reflection,

$$\int_{-k}^{k}\beta(\alpha)R_1(\alpha)I_2(-\alpha)d\alpha = \int_{-k}^{k}\beta(\alpha)R_2(-\alpha)I_1(\alpha)d\alpha, \quad \text{(B4)}$$

where $I_1(\alpha)$ and $I_2(\alpha)$ are the spectral distributions for two different realizations of the incident field, and $R_1(\alpha)$ and $R_2(\alpha)$ are the corresponding backward diffracted spectral distributions. Using Eq. (9) or Eq. (24a) and the explicit expressions for the specific realizations of the field given by Eq. (A3) according to the case, one gets

$$I_1(\alpha) = \sum_{j=1}^{N}\sqrt{2\pi}U_j^{(1)}e^{i\eta_j^{(1)}}\delta(\alpha - k\sin\theta_j^{(1)})e^{i[\beta(\alpha)-k\cos\theta_j^{(1)}]y}, \quad \text{(B5)}$$

$$I_2(\alpha) = \sum_{j'=1}^{N'}\sqrt{2\pi}U_{j'}^{(2)}e^{i\eta_{j'}^{(2)}}\delta(\alpha - k\sin\theta_{j'}^{(2)})e^{i[\beta(\alpha)-k\cos\theta_j^{(2)}]y}. \quad \text{(B6)}$$

Thus, the reciprocity relation can be written in the form

$$\sum_{j=1}^{N}U_j^{(1)}e^{i\eta_j^{(1)}}\cos\theta_j^{(1)}T_2(-k\sin\theta_j^{(1)}) = \sum_{j\prime=1}^{N'}U_{j'}^{(2)}e^{i\eta_{j'}^{(2)}}\cos\theta_{j'}^{(2)}T_1(-k\sin\theta_{j'}^{(2)}). \quad \text{(B7)}$$

Here, T_s represents the upwardly diffracted spectral distibution corresponding to the incident field whose spectral distribution is I_s, $s=1,2$.

[1] Lord Rayleigh, Proc. R. Soc. London **A79**, 399 (1907).
[2] C. J. Bouwkamp, Rep. Prog. Phys. **17**, 35 (1954).
[3] J. B. Keller, J. Appl. Phys. **28**, 426 (1957).
[4] K. Hongo and G. Ishii, IEEE Trans. Antennas Propag. **AP–26**, 494 (1978).
[5] O. Mata-Méndez, M. Cadilhac, and R. Petit, J. Opt. Soc. Am. **73**, 328 (1983).
[6] B. Hafizi and P. Sprangle, J. Opt. Soc. Am. A **8**, 705 (1991).
[7] P. L. Overfelt and C. S. Kenney, J. Opt. Soc. Am. A **8**, 732 (1991).
[8] O. Mata-Méndez and F. Chávez-Rivas, J. Opt. Soc. Am. A **12**, 2440 (1995).
[9] O. Mata-Méndez and F. Chávez-Rivas, J. Opt. Soc. Am. A **18**, 537 (1993).
[10] F. Montiel and M. Nevière, Opt. Commun. **101**, 151 (1993).
[11] P. O'Connor, J. Gehlen, and E. J. Heller, Phys. Rev. Lett. **58**, 1296 (1987).
[12] E. J. Heller, in *Chaos and Quantum Physics*, edited by M. J. Giannoni, A. Voros, and J. Zinn-Justin, Les Houches, Session LII (Elsevier, New York, 1989).
[13] O. Mata-Méndez and F. Chávez-Rivas, Rev. Mex. Fis. **39**, 371 (1993).
[14] D. Maystre, in *Rigorous Vector Theories of Diffraction Gratings*, edited by E. Wolf, Progress in Optics (North Holland,

Amsterdam, 1984).
[15] R. Petit, in *Electromagnetic Theory of Gratings*, edited by R. Petit, Topics in Current Physics Vol. 22 (Springer-Verlag, Berlin, 1980), p. 1.
[16] We are using the expression *diffraction of the incident wave* as is customary in the study of diffraction problems in optics, that is, as referring to an input wave. This differs from the usage in scattering theory, where input wave refers to a free wave solution to the scattering problem and, thus, contains both ingoing and outgoing components.
[17] M. Cadilhac, in *Electromagnetic Theory of Gratings*, edited by R. Petit, Topics in Current Physics Vol. 22 (Springer-Verlag, Berlin, 1980), p. 53.
[18] D. Maystre, O. Mata-Méndez, and A. Roger, Opt. Acta **30**, 1707 (1983).
[19] O. Mata-Méndez, Phys. Rev. B **37**, 8182 (1988).
[20] L. de la Peña and A. M. Cetto, *The Quantum Dice. An Introduction to Stochastic Electrodynamics* (Kluwer Academic Publisher, Netherlands, 1996).
[21] T. H. Boyer, Phys. Rev. D **11**, 790 (1975); **11**, 809 (1975).
[22] T. H. Boyer, Phys. Rev. A **18**, 1228 (1978).
[23] L. de la Peña and A. M. Cetto, Found. Phys. **31**, 1703 (2001); quant-ph/0501011 (unpublished).
[24] P. W. Milonni, *The Quantum Vacuum: An Introduction to Quantum Electrodynamics* (Academic Press, San Diego, 1994).
[25] M. Ibison and B. Haisch, Phys. Rev. A **54**, 2737 (1996).